Nanoscale Advances

ROYAL SOCIETY OF CHEMISTRY

PAPER

View Article Online
View Journal | View Issue

Cite this: *Nanoscale Adv.*, 2024, **6**, 2636

Anomalous spectral shift of localized surface plasmon resonance†

Saikiran Kosame,[a] Mukkath Joseph Josline,[bc] Jae-Hyun Lee [bc] and Heongkyu Ju *[a]

We report the first observation of spectral blue shift of plasmon resonance of synthesized silver nanoparticles (AgNPs) due to a negative optical nonlinearity of a local ambient medium, *i.e.*, indigo carmine (IC) solution at around 420 nm wavelength. The blue shift occurred at a larger concentration of AgNPs or at a larger concentration of IC solution, being in obvious contrast to spectral red shift which was widely witnessed in plasmon spectral shift in a linear regime. Plasmon-enhanced local fields could excite the third-order optical nonlinearity for blue shift even under continuous (non-pulsed) light illumination. We also found that the plasmon-excited nonlinearity could allow for differential nonlinear response of the IC solution to be even greater than its differential linear response, though appearing to be somewhat inconsistent with what was generally known in light–matter interaction. The demonstrated properties of such anomalous shift of plasmon spectral peaks and its accompanying properties indicated that plasmon technologies could be exploited not only in linear but also in nonlinear aspects for critical optimization in plasmon-energy harvesting systems such as in surface enhanced spectroscopy/microscopy, biomedical imaging/sensing, laser frequency conversion, ultrashort pulse generation, and all-optical switching.

Received 19th December 2023
Accepted 3rd April 2024

DOI: 10.1039/d3na01131c

rsc.li/nanoscale-advances

1. Introduction

Localized surface plasmon resonance (LSPR) arises from the coherently coupled mode between collective oscillation of conduction electrons and electric fields of incident electromagnetic (EM) radiation at metal–dielectric interfaces.[1–6] Nanoscaled metallic structures enable surface-parallel momentum (phase) matching between incident EM fields and surface plasmons. Noble metals such as gold (Au) and silver (Ag) provide nanomaterial platforms for the dispersion relation of local plasmons to be tuned at visible and near infrared wavelengths. A dielectric medium that forms an interface with a metallic nanostructure, such as liquid solvent in colloidal Ag nanoparticles (AgNPs), plays a role in determining the wavelength (frequency) of LSPR. A larger refractive index of the dielectric medium leads to longer wavelengths (smaller frequencies) of LSPR due to dielectric screening effects,[7–10] *i.e.*, spectral red shift of LSPR. This spectral red shift has been widely exploited for applications in chemical and biological sensing due to its high sensitivity to refractive index change in ambient dielectric medium surrounding the metallic nanostructures.[1–3,7,9]

One of the intriguing benefits of LSPR is the confinement of radiation energy within sub-diffraction-limited volume near the surface of metallic nanostructures, producing local enhancement of photonic density. This local field enhancement could boost the optical nonlinearity of the ambient dielectric medium or metal itself for various applications including surface enhanced Raman spectroscopy,[11–13] second harmonic generation,[14–17] all-optical signal processing,[18,19] and ultrashort pulse generation.[20–22]

In this work, we studied the LSPR-boosted nonlinear effects of colloidal AgNPs using absorbance spectroscopy in the visible wavelength region. AgNPs synthesized using β-cyclodextrin (β-CD) as a stabilizing/reducing agent were made into colloids with various solvents such as water, solution of *N*-dimethyl formamide (DMF) and solution of indigo carmine (IC). We adopted IC as a nonlinear medium due to its large third-order optical nonlinearity at visible wavelengths.[23–25] Absorbance spectroscopy of colloidal AgNPs demonstrated the spectral blue shift of plasmonic peaks with increasing AgNP concentration only when IC solution was used as solvent. For a given AgNP concentration, the blue shift was also observed when increasing IC concentration, which was in contrast to the spectral peak red shift of LSPR typically observed when increasing the concentration of an ambient medium. These abnormal phenomena were due to the negative optical Kerr effects that arose from IC

[a]*Department of Physics, Gachon University, Seongnam-si 13120, Republic of Korea. E-mail: batu@gachon.ac.kr*

[b]*Department of Materials Science and Engineering, Ajou University, Suwon, Korea*

[c]*Department of Energy Systems Research, Ajou University, Suwon, Korea*

† Electronic supplementary information (ESI) available. See DOI: https://doi.org/10.1039/d3na01131c

third-order optical nonlinearity enhanced by plasmon-induced local field enhancement. We provided detailed discussion with analysis of plasmon spectral peak shift, which could be split into linear and nonlinear ones to understand such anomalous spectral shift.

2. Materials

2.1 Chemical components

IC, a blue-colored dye with a molecular weight of 466.35 Dalton, silver nitrate ($AgNO_3$), sodium hydroxide (NaOH), DMF, and β-CD were purchased from Sigma-Aldrich (Rahway, NJ, USA). Double-distilled water was used as a solvent to dissolve IC powder under ultra-sonication for 30 minutes into IC solutions of various concentrations, *i.e.*, 0.05, 0.1, 0.2, 0.3, 0.4, 0.5, and 0.6 mM. All other reagents used in this study were of analytical reagent grade.

2.2 Synthesis of colloidal AgNPs

Fig. 1 shows the schematic for the synthesis of AgNPs using β-CD as a stabilizing agent.[26] The cyclic oligosaccharide β-CD (0.396 g) was mixed with 49 mL of water and stirred until the mixture became transparent. NaOH (1 M, 0.5 mL) was then added to the solution to maintain its pH at ∼11. After 2 minutes, 0.6 mL of 10 mM $AgNO_3$ was added dropwise to the solution.

The final mixture was placed in a water bath at 80 °C for 20 min to ensure an efficient reaction. The colorless-to-yellow change indicated the formation of AgNPs, which was further verified by high-resolution transmission electron microscopy (HR-TEM) (JEM-2100, JEOL Ltd, Japan). Colloidal AgNPs were made with two types of dispersion media, *i.e.*, IC solution or DMF for various concentrations using a magnetic stirrer for 5 min. The absorbance of the colloidal AgNPs in IC solution was characterized with a UV-VIS spectrophotometer (Ultra-3660 series, Rigol, USA) with a spectral resolution of 0.5 nm (visible wavelengths) to investigate spectral plasmon resonance.

The interaction of IC molecules and AgNPs could be made through the hollow truncated structures of β-CD, where the inner part was hydrophobic while the outer part was hydrophilic (–OH) as seen in Fig. S1.† The fac that IC molecules-AgNP interaction did not lead to substantial change in the AgNP size was confirmed by X-ray diffraction measurement (XRD) and X-ray photoelectron spectroscopy (XPS) as follows. The XRD results obtained with freeze drying of AgNPs showed characteristic peaks at 37.6° (111) and at 44.3° (200)[27] that remained unchanged between both cases of before and after addition of IC molecules (β-cyclodextrin has characteristic peak positions at 12°, 17° and 35°)[28] as shown in Fig. S2.† In addition, the XPS results obtained using AgNPs in both cases produced oxidation states at 373.5 eV and 367.5 eV of Ag,[29] which remained unchanged as seen in Fig. S3.†

3. Results and discussion

3.1 Morphology of AgNPs

For HR-TEM images of AgNPs, 1 mL of colloidal AgNP solution was sonicated for 10 min and deposited on a copper grid, followed by heat treatment in an oven at 60 °C to evaporate the solvent. Then HR-TEM images were taken and processed using Image J software to obtain AgNPs' morphological structure including particle size information. Fig. 2(a) shows the HR-TEM image of the AgNPs, revealing the nearly spherical shape of AgNPs. The inset of Fig. 2(a) provides the SAED pattern of AgNPs with clear Debye–Scherrer rings, which indicate their crystallinity. The size of AgNPs was estimated to be 8 ± 2 nm.

3.2 Spectral red shift of plasmons and its sensitivity to an ambient refractive index

To investigate the spectral peak shift of the plasmon resonance peak of colloidal AgNPs with absorbance spectroscopy, DMF solutions of various concentrations were used as solvent for colloids. Increasing the concentration (volume-to-volume ratio) from 0% (DI water) to 100% (pure DMF) in steps of 10% made the (linear) refractive index of the ambient medium around AgNPs increase linearly, producing the spectral red-shift of the LSPR peak (maximum shift of ∼14 nm at 100%), as shown in Fig. 3(a). In addition, the fact that the absorbance at the plasmonic resonance increased with increasing DMF concentration was attributed to the properties of dipole scattering of AgNPs.[30] Meanwhile, to estimate the sensitivity of the spectral peak shift of AgNP LSPR to change in an ambient medium refractive index, we measured independently the refractive index of DMF solution *versus* its concentration using an Abbe refractometer (DR-A1; Attago, Tokyo, Japan). The linear relationship between them was fitted ($R^2 = 0.992$) with the linear regression of $n = 1.3295 + 0.00104C$, where n is the refractive index of DMF at its concentration. Fig. 3(b) shows the spectral red shift *versus*

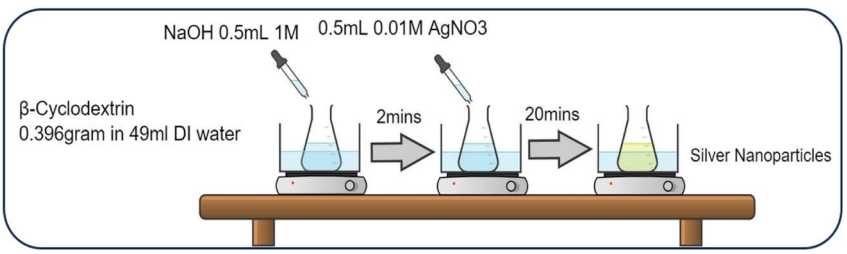

Fig. 1 Synthesis procedure for AgNPs.

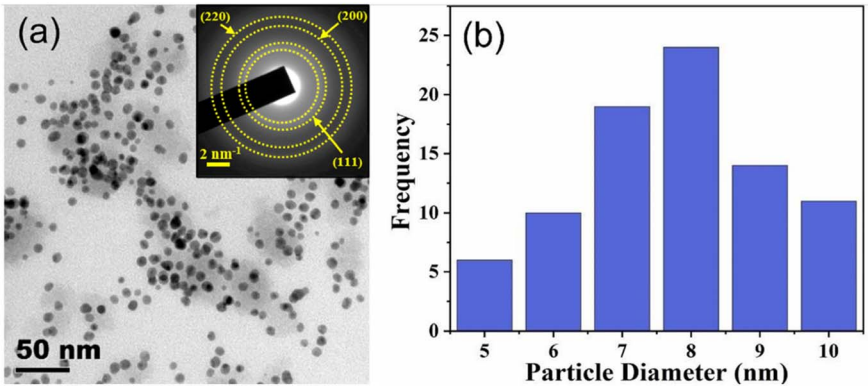

Fig. 2 (a) HR-TEM image of AgNPs. The inset shows the SAED pattern where the lattice planes of AgNPs which correspond to the Debye–Scherrer rings are added. (b) Particle size distribution.

a refractive index of an ambient medium for AgNPs. The plots exhibited a monotonically increased red shift as the refractive index increased. The sensitivity defined as $S \equiv \Delta\lambda/\Delta n$, where $\Delta\lambda$ and Δn are the spectral peak shift and the index change, respectively, was then estimated to be ~131.6 nm per RIU. The above-defined S represented the effective sensitivity, taking into account the characteristic decay length of local fields,[7] and thus assumed linearity between them though slight nonlinear digression was present in the range.

3.3 Plasmon spectral blue shift of colloidal AgNPs

First, we arranged colloidal AgNPs of various concentrations, *i.e.*, from 3 nM to 48 nM, in a step of 3 nM using DI water as solvent to measure their absorbance spectra. This was to check if there occurred spectral shift due to a possibility that the ambient refractive index around AgNPs might have changed *via* an increased density of AgNPs within local ambient medium around AgNPs. Fig. 4(a) shows that the absorbance spectral peak remained nearly unchanged even if AgNP concentration was increased. The fact that DI water was not optically nonlinear manifested negligible change in the effective index of an ambient medium near AgNPs despite possible plasmonic enhancement of local fields around the particles. This also would indicate a possibility that, under light illumination, the interparticle distance would have been much longer than the dimension of local dielectric space near AgNPs, into which plasmonic evanescent fields would have been penetrated.

We replaced DI water by IC solutions for solvent of colloidal AgNPs and measured the effective refractive index *versus* AgNP concentration for various concentrations of IC solutions, using an Abbe refractometer (DR-A1; Attago, Tokyo, Japan). Negligible dependence of the effective index of colloids on AgNP concentration was observed for all concentrations of IC solution, as shown in Fig. 4(b). This revealed that increasing concentration of AgNPs did not change significantly the effective linear refractive index of the colloidal AgNPs (with solvent of IC solution).

Given the above-mentioned properties of an effective linear index of the colloidal AgNPs, we performed their absorbance

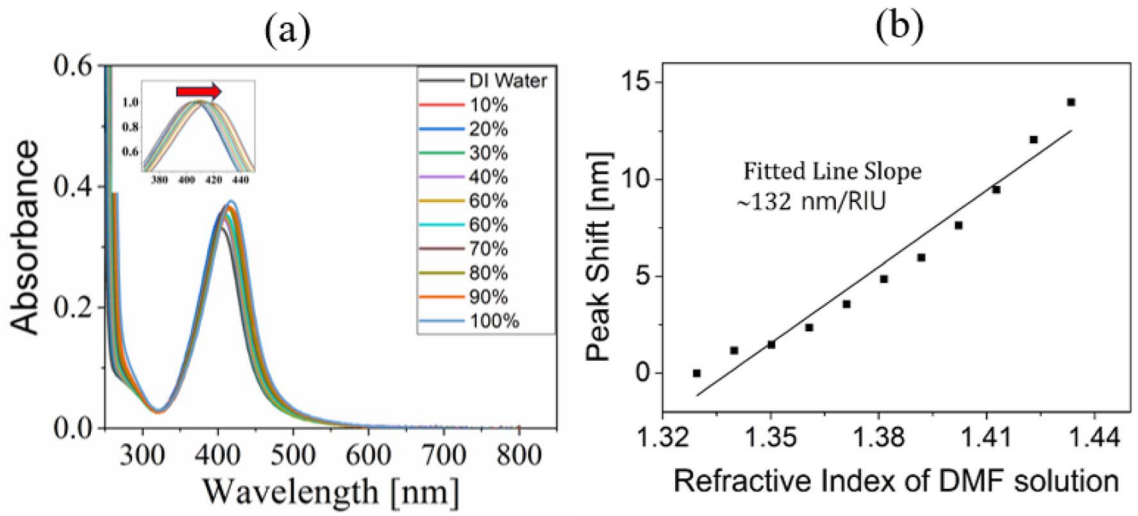

Fig. 3 (a) Absorbance spectroscopy of colloidal AgNPs (100 μM) when using DMF solution of various concentration as colloidal solvent. (b) Spectral peak shift of the AgNP absorbance peak *versus* refractive index of a DMF concentration with linear regression.

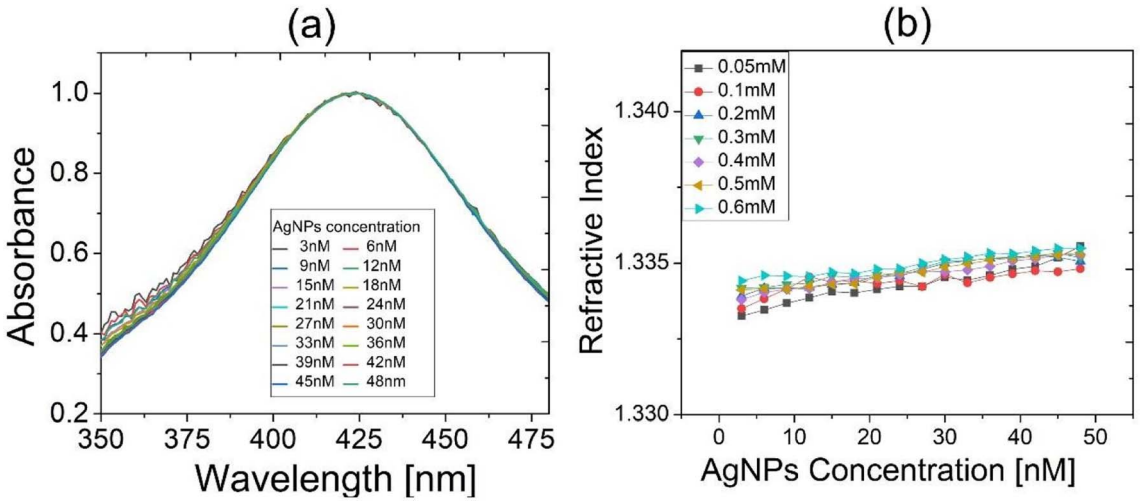

Fig. 4 (a) Absorbance spectroscopy of colloidal AgNPs at various concentrations (water as colloid solvent). (b) The measured linear refractive index (n_L) of AgNP colloids (IC solution as solvent) *versus* AgNP concentration for various concentrations of IC solution. An Abbe refractometer was used to measure them.

spectroscopy for various IC concentrations to examine the shift of the plasmon spectral peak when increasing the AgNP concentration. Each absorbance spectrum data point was normalized with respect to the respective plasmon spectral peak that occurred at around 400–420 nm. For all IC concentrations, the blue shift of the plasmon spectral peaks (shift towards shorter wavelengths) was observed when increasing AgNP concentration, as shown in Fig. 5(a)–(f). This apparently differed from the cases of nearly no peak shift shown in Fig. 4(a) for which DI water was used as solvent for colloidal AgNPs.

Meanwhile, the blue shift of the spectral peaks was even enhanced for larger IC concentration as seen in Fig. 6(a). Accordingly, the fact that larger concentrations of IC solution produced the bluer shift of spectral peaks appeared to contradict the fact that a larger concentration of DMF solution produced the red shift of spectral peaks in terms of the plasmon peak shift direction (see Fig. 3(a)). It was worth noting that another spectral peak at ~610 nm (not shown in Fig. 5(a)–(f) but shown in Fig. S4†) made no shift at all when increasing the concentration of AgNPs or IC solutions no matter what solvent was used (DMF or IC solution). This indicated that the spectral peak at ~610 nm did not arise from the plasmons of AgNPs but from the characteristic absorbance of IC.[23,24]

Regarding the mechanism of the unusual direction of plasmon peak shift, *i.e.*, blue shift, we excluded the possibility of AgNP assembly formation because it generally produced the spectral red shift.[31] Meanwhile, the charge transfer between AgNPs might account for the presence of the blue shift.[32] However, the colloidal form of AgNPs where the interparticle distance was much longer than a wavelength of incident light would not serve for the nano-scaled bridge through which charge transfer could occur. Conversely, such blue shift of plasmon spectral peaks could be explained by the negative nonlinear refractive index of IC solution, which formed an ambient local medium around AgNPs. This was because IC third-order optical nonlinearity was activated by plasmon-enhanced local fields around AgNPs at 400–420 nm. Previously, the third-order optical nonlinearity of IC was demonstrated as negative nonlinearity at around 405 nm in an optical Z-scan experiment, where the high intensity of picosecond pulsed light enabled its excitation.[24] In this work, enhanced local fields around plasmonic AgNPs were substituted for the high intensity of the picosecond pulsed light, to excite such negative third-order nonlinearity.

The blue shift that occurred at larger IC concentrations or at larger AgNP concentrations as shown in Fig. 6(a) could be considered as net shift of the peak wavelength ($\Delta\lambda_{net}$) resulting from two contributions at larger concentrations, the red shift of the peak wavelength ($\Delta\lambda_L > 0$) induced by increase in the linear refractive index (n_L) and the blue shift ($\Delta\lambda_{NL} < 0$) induced by increase in the negative nonlinear index ($n_{NL} < 0$), as given by

$$\Delta\lambda_{net} = \Delta\lambda_L + \Delta\lambda_{NL} \quad (1)$$

For a given concentration of AgNPs and IC solution, the net refractive index of colloids is given by

$$n_{net} = n_L + n_{NL} \quad (2)$$

Here n_L is the effective index of linear refraction, and $n_{NL} = n_2 I$ is the effective index of nonlinear refraction of the AgNP colloid, where n_2 is the optical Kerr coefficient. The optical intensity (I) dependence of a refractive index was governed by the third-order optical nonlinearity under optical Kerr effects. Our group previously reported $n_2 \sim -1.0 \times 10^{-7}$ cm^2 W^{-1} of IC solutions (~1 mM) at 405 nm, which was higher than those of silica fibers or inorganic semiconductors, and its large magnitude was due to delocalized π electrons in the aromatic conjugation structure of IC molecules. It was also noted that n_2 was negative at near 405 nm,[23–25] which was close to the AgNP plasmon wavelengths (400–420 nm) of the current studies.

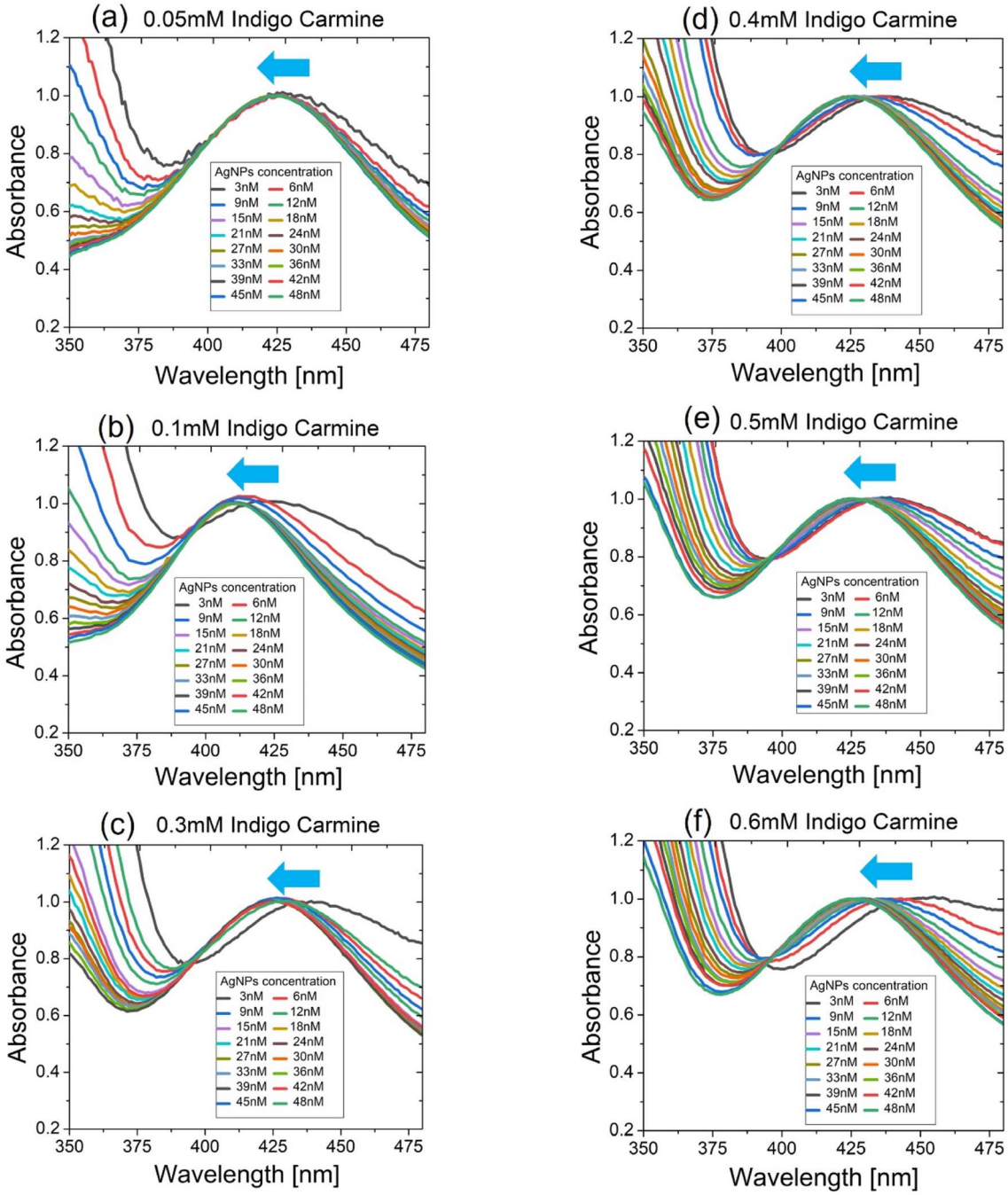

Fig. 5 The blue shift of the absorbance spectral peaks of colloidal AgNPs for which indigo carmine (IC) solution was used as solvent. IC concentrations were 0.05 mM (a), 0.1 mM (b), 0.3 mM (c), 0.4 mM (d), 0.5 mM (e), and 0.6 mM (f).

When increasing the AgNP concentration in colloids, the plasmon-enhanced intensity of local fields near AgNPs enhanced n_{NL} (<0) due to its intensity dependence, while n_L remained nearly unchanged as shown in Fig. 4(b). For all IC concentrations, this enhancement of n_{NL} *i.e.*, Δn_{NL} produced the blue shift when increasing the AgNP concentration until about 20 nM concentration, beyond which it saturated as shown in Fig. 6(a). It was also found that such a blue shift was greater at larger concentrations of IC solutions for a given concentration of AgNPs, indicating the clear manifestation of the negative nonlinearity of IC solutions that played a significant role in the anomalous spectral peak shift.

Fig. 6(b) shows the maximum blue shift of a spectral peak that occurs at the maximum AgNP concentration (48 nM), as a function of IC concentration (solvent). The plasmonic peak sensitivity to an ambient refractive index change, *i.e.*, $S \sim 132$ nm per RIU obtained above (see Fig. 3(b)), enabled us to estimate, at an IC concentration of 0.6 mM, the nonlinear refractive

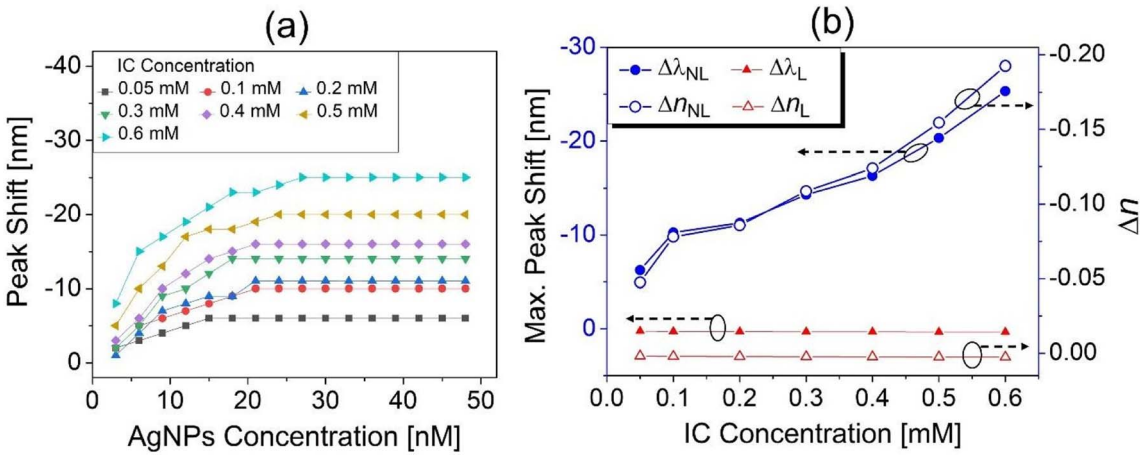

Fig. 6 (a) Plasmon spectral peak shift *versus* AgNP concentration for various IC concentrations. (b) Spectral peak shift and the corresponding nonlinear refractive index change (Δn) as a function of IC concentration at an AgNP concentration of 48 nM (thus the maximum peak shift and Δn).

index changes as $\Delta n_{NL} \cong -0.19$ from the measured maximum blue shift of $\Delta\lambda_{net} = -25$ nm. For this estimation of Δn_{NL}, eqn (1) and (2) were used with both the measured values of n_L (shown in Fig. 4(b)) and the correspondingly estimated linear red shift of a spectral peak, *i.e.*, $\Delta\lambda_L = S\,(n_L - n_{water})$. It was worth noting that the magnitude of Δn_{NL} was surprisingly far greater than Δn_L, so was that of $\Delta\lambda_{NL}$ than that of $\Delta\lambda_L$ as shown in Fig. 6(b). This could appear to be somewhat contradictory to the general optical properties that a linear response of a medium such as the refractive index was always much greater, in magnitude, than its nonlinear response at a given wavelength. However, in this work, focus was placed not on the refractive indices themselves (*i.e.*, n_L and n_{NL}) but on their change (*i.e.*, Δn_L and Δn_{NL}) under the influence of AgNP plasmon-enhanced local fields that greatly enhanced the nonlinear response. These intriguing properties led to an expectation that the differential response of materials to electric field stimuli achieved by nonlinear plasmon technologies could be exploited for applications that deal with incremental signal change, such as in biomolecular/biochemical sensor technologies and the relevant imaging technologies.

3.4 Simulation of plasmon local field enhancement

To investigate the electric field distribution close to the AgNP surface, numerical modelling and three-dimensional finite difference time domain (3D FDTD) calculations were carried out using a commercial program (Ansys Lumerical FDTD, Ansys, USA). A total field scattered field (TFSF) light source was used. A frequency domain monitor was applied for evaluating and visualizing the final *E*-field enhancement. Material and optical parameters used in the calculation included the experimentally measured values such as the average size of spherical AgNPs (8 ± 2 nm obtained from the HR-TEM image) and the refractive indices of solvents (from Abbe refractometer measurement). The complex dielectric constant of Ag found in the literature[33] was also used in the calculation. The incident light wavelength was varied from λ = 200 to 800 nm to find the plasmonic resonance wavelength. The mesh step was set to a minimum, *i.e.*, 0.1 nm for a given limited computation capacity. As shown in Fig. 7, the calculation of local electric fields around a single nano-particle exhibited the highest enhancement (more than 10-fold) over incident fields at a wavelength of 405 nm among

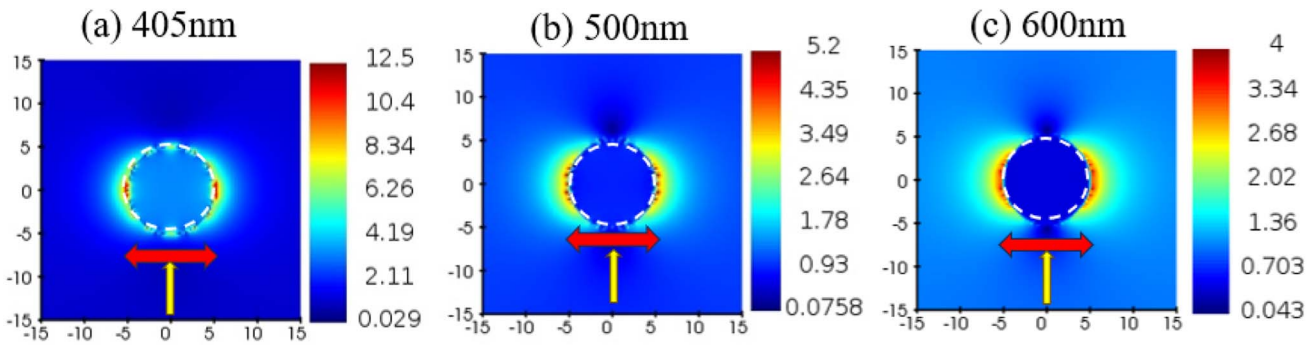

Fig. 7 Numerical simulation of electric field strength $|(x, y)|^2$ around AgNPs at the wavelengths of 405 nm (a), 500 nm (b) and 600 nm (c). Here (x, y) is the electric field as a function of horizontal and vertical coordinates in nanometres (x and y). Yellow and red arrows denote the incident light direction and its polarization, respectively. White dashed lines represent the AgNP boundary.

all the wavelengths probed, corresponding to the LSPR wavelength.

4. Conclusions

We demonstrated the blue shift of surface plasmon spectral peaks of AgNPs when increasing the concentration of an ambient dielectric medium, the first observation of such anomalous shift to the best of our knowledge. The ambient dielectric medium was an IC solution that interacted non-linearly with the plasmon-enhanced local fields near AgNPs under (non-pulsed) continuous wave light illumination. This accounted for such a blue shift of plasmon resonance *via* negative optical Kerr effects that exhibited the intensity dependence of the nonlinear refractive index, *i.e.*, $n_{NL} = n_2 I$ ($n_2 < 0$).

More interestingly, as the IC concentration increased, incremental change in nonlinear effects, *i.e.*, magnitude of nonlinear blue shift turned out to be much greater than that in linear effects such as the magnitude of linear red shift. This appeared to be somewhat in disagreement with a general feature in light–matter interaction, *i.e.*, a linear response of the material to a stimulus such as an externally applied electric field would be much greater than its nonlinear response. However, the properties demonstrated in this study showed possibility that differential nonlinear response could be much greater than differential linear response when using plasmon-induced enhancement of local fields that were made to interact with a nonlinear medium. These features need to be critically considered particularly in optoelectronic devices that harvest plasmon energy with optical parameters required to be fine-tuned such as those that employed surface enhanced spectroscopy/microscopy, biomedical sensing/imaging and nonlinear plasmonics.

Conflicts of interest

There are no conflicts to declare.

Acknowledgements

This work was supported by the Gachon University research fund of 2021 (GCU-202110320001), and also supported by the National Research Foundation of Korea (NRF) grant funded by the Korean government (MSIT) (No. RS-2023-00279149).

References

1 E. Petryayeva and U. J. Krull, Localized surface plasmon resonance: Nanostructures, bioassays and biosensing-A review, *Anal. Chim. Acta*, 2011, **706**(1), 8–24, DOI: 10.1016/j.aca.2011.08.020.

2 K. A. Willets and R. P. Van Duyne, Localized surface plasmon resonance spectroscopy and sensing, *Annu. Rev. Phys. Chem.*, 2007, **58**, 267–297, DOI: 10.1146/annurev.physchem.58.032806.104607.

3 E. Hutter and J. H. Fendler, Exploitation of localized surface plasmon resonance, *Adv. Mater.*, 2004, **16**(19), 1685–1706, DOI: 10.1002/adma.200400271.

4 M. M. Miller and A. A. Lazarides, Sensitivity of metal nanoparticle surface plasmon resonance to the dielectric environment, *J. Phys. Chem. B*, 2005, **109**(46), 21556–21565, DOI: 10.1021/jp054227y.

5 T. R. Jensen, M. D. Malinsky, C. L. Haynes and R. P. Van Duyne, Nanosphere lithography: Tunable localized surface plasmon resonance spectra of silver nanoparticles, *J. Phys. Chem. B*, 2000, **104**(45), 10549–10556, DOI: 10.1021/jp002435e.

6 S. Kaushal, S. S. Nanda, D. K. Yi and H. Ju, Effects of Aspect Ratio Heterogeneity of an Assembly of Gold Nanorod on Localized Surface Plasmon Resonance, *J. Phys. Chem. Lett.*, 2020, **11**(15), 5972–5979, DOI: 10.1021/acs.jpclett.0c01507.

7 A. J. Haes, D. A. Stuart, S. Nie and R. P. Van Duyne, Using Solution-Phase Nanoparticles, Surface-Confined Nanoparticle Arrays and Single Nanoparticles as Biological Sensing Platforms, *J. Fluoresc.*, 2004, **14**, 355–367, DOI: 10.1023/B:JOFL.0000031817.35049.1f.

8 A. J. Haes, S. Zou, J. Zhao, G. C. Schatz and R. P. Van Duyne, Localized surface plasmon resonance spectroscopy near molecular resonances, *J. Am. Chem. Soc.*, 2006, **128**(33), 10905–10914, DOI: 10.1021/ja063575q.

9 J. S. Seok and H. Ju, Plasmonic optical biosensors for detecting c-reactive protein: A review, *Micromachines*, 2020, **11**(10), 0895, DOI: 10.3390/mi11100895.

10 M. Piliarik, P. Kvasnička, N. Galler, J. R. Krenn and J. Homola, Local refractive index sensitivity of plasmonic nanoparticles, *Opt. Express*, 2011, **19**, 9213–9220, DOI: 10.1364/OE.19.009213.

11 K. Kneipp, Y. Wang, H. Kneipp, L. T. Perelman, I. Itzkan, R. R. Dasari and M. S. Feld, Single Molecule Detection Using Surface-Enhanced Raman Scattering (SERS), *Phys. Rev. Lett.*, 1997, **78**, 1667–1670, DOI: 10.1103/PhysRevLett.78.1667.

12 S. Nie and S. R. Emory, Probing single molecules and single nanoparticles by surface-enhanced Raman scattering, *Science*, 1997, **275**(5303), 1102–1106, DOI: 10.1126/science.275.5303.1102.

13 E. C. Le Ru, E. Blackie, M. Meyer and P. G. Etchegoint, Surface enhanced Raman scattering enhancement factors: A comprehensive study, *J. Phys. Chem. C*, 2007, **111**(37), 13794–13803, DOI: 10.1021/jp0687908.

14 F. W. Vance, B. I. Lemon and J. T. Hupp, Enormous hyper-Rayleigh scattering from nanocrystalline gold particle suspensions, *J. Phys. Chem. B*, 1998, **102**(50), 10091–10093, DOI: 10.1021/jp984044u.

15 J. Nappa, I. Russier-Antoine, E. Benichou, C. Jonin and P. F. Brevet, Second harmonic generation from small gold metallic particles: From the dipolar to the quadrupolar response, *J. Chem. Phys.*, 2006, **125**(18), 184712, DOI: 10.1063/1.2375095.

16 S. Wunderlich and U. Peschel, Plasmonic enhancement of second harmonic generation on metal coated

nanoparticles, *Opt. Express*, 2013, **21**(16), 18611, DOI: 10.1364/oe.21.018611.

17 M. Chandra and P. K. Das, "Small-particle limit" in the second harmonic generation from noble metal nanoparticles, *Chem. Phys.*, 2009, **358**(3), 203–208, DOI: 10.1016/j.chemphys.2009.02.003.

18 G. A. Wurtz and A. V. Zayats, Nonlinear surface plasmon polaritonic crystals, *Laser Photonics Rev.*, 2008, **2**(3), 125–135, DOI: 10.1002/lpor.200810006.

19 G. A. Wurtz, *et al.*, Designed ultrafast optical nonlinearity in a plasmonic nanorod metamaterial enhanced by nonlocality, *Nat. Nanotechnol.*, 2011, **6**(2), 107–111, DOI: 10.1038/nnano.2010.278.

20 R. A. Ganeev, R. I. Tugushev and T. Usmanov, Application of the nonlinear optical properties of platinum nanoparticles for the mode locking of Nd:glass laser, *Appl. Phys. B*, 2009, **94**(4), 647–651, DOI: 10.1007/s00340-009-3371-9.

21 T. Jiang, Y. Xu, Q. Tian, L. Liu, Z. Kang, R. Yang, G. Qin and W. Qin, Passively Q-switching induced by gold nanocrystals, *Appl. Phys. Lett.*, 2012, **101**(15), 151122, DOI: 10.1063/1.4759120.

22 Z. Ma, *et al.*, Composite film with anisotropically enhanced optical nonlinearity for a pulse-width tunable fiber laser, *J. Mater. Chem. C*, 2018, **6**(5), 1126–1135, DOI: 10.1039/c7tc03711b.

23 S. Pramodini and P. Poornesh, Third-order nonlinear optical response of indigo carmine under 633 nm excitation for nonlinear optical applications, *Opt. Laser Technol.*, 2014, **63**, 114–119, DOI: 10.1016/j.optlastec.2014.04.007.

24 J. Hong and H. Ju, Ultrafast Third-Order Optical Nonlinearity of Indigo Carmine Excited by Pico-second Pulsed Laser at 405 nm, *New Phys.: Sae Mulli*, 2023, **73**(2), 165–172, DOI: 10.3938/npsm.73.165.

25 J. Hong and H. Ju, All-optical modulation by continuous wave light using two-color excited state absorption at visible wavelengths, *Opt. Lett.*, 2024, **49**(1), 157–160, DOI: 10.1364/OL.504161.

26 R. Rajamanikandan and M. Ilanchelian, β-cyclodextrin functionalised silver nanoparticles as a duel colorimetric probe for ultrasensitive detection of Hg2+ and S2− ions in environmental water samples, *Mater. Today Commun.*, 2018, **15**, 61–69, DOI: 10.1016/j.mtcomm.2018.02.024.

27 K. Yang, J. Liu, L. Luo, M. Li, T. Xu and J. Zan, Synthesis of cationic *β*-cyclodextrin functionalized silver nanoparticles and their drug-loading applications, *RSC Adv.*, 2023, **13**(11), 7250–7256, DOI: 10.1039/d2ra08216k.

28 R. N. Patil and A. V. Kumar, Unprecedented concomitant formation of Cu_2O-CD nano-superstructures during the aerobic oxidation of alcohols and their catalytic use in the propargyl amination reaction: A simultaneous catalysis and metal waste valorization (SCMWV) Method, *ACS Omega*, 2017, **2**(10), 6405–6414, DOI: 10.1021/acsomega.7b00898.

29 G. Lin, C. Zhao, W. Liao, J. Yang and Y. Zheng, Eco-Friendly Green Synthesis of Rubropunctatin Functionalized Silver Nanoparticles and Evaluation of Antibacterial Activity, *Nanomaterials*, 2022, **12**(22), 4052, DOI: 10.3390/nano12224052.

30 S. Link and M. A. El-Sayed, Spectral Properties and Relaxation Dynamics of Surface Plasmon Electronic Oscillations in Gold and Silver Nanodots and Nanorods, *J. Phys. Chem. B*, 1999, **103**(40), 8410–8426, DOI: 10.1021/jp9917648.

31 L. Catanzaro, V. Scardaci, M. Scuderi, M. Condorelli, L. D'Urso and G. Compagnini, Surface plasmon resonance of gold nanoparticle aggregates induced by halide ions, *Mater. Chem. Phys.*, 2023, **308**, 128245, DOI: 10.1016/j.matchemphys.2023.128245.

32 A. N. Koya and J. Lin, Charge transfer plasmons: Recent theoretical and experimental developments, *Appl. Phys. Rev.*, 2017, **4**, 021104, DOI: 10.1063/1.4982890.

33 P. B. Johnson and R. W. Christy, Optical constants of the noble metals, *Phys. Rev. Lett.*, 1972, **11**, 4370–4379, DOI: 10.1103/PhysRevB.6.4370.